Pramana – J. Phys. (2019) 93:41
https://doi.org/10.1007/s12043-019-1797-0

An analytical approach to the metal and metallic oxide properties of Cu–water and TiO_2–water nanofluids over a moving vertical plate

B C ROUT and S R MISHRA*

Department of Mathematics, Siksha 'O' Anusandhan Deemed to be University, Khandagiri, Bhubaneswar 751 030, India
*Corresponding author. E-mail: satyaranjan_mshr@yahoo.co.in

MS received 26 September 2018; revised 11 February 2019; accepted 20 February 2019; published online 19 June 2019

Abstract. An analysis was carried out to study the flow phenomena of an unsteady, electrically conducting, water-based nanofluid embedded with a porous matrix over a moving/stationary plate. The effects on the nanofluid flow were observed by taking copper (Cu) and titanium oxide (TiO_2) nanoparticles. The crux of the investigation is to examine the influence of thermal radiation, radiation absorption parameter accounted for in the energy equation. The first-order chemical reaction was also taken care of by incorporating it into the solutal transfer equation. Closed form solution holds good for nonlinear coupled partial differential equations. Solutions of these equations are obtained by employing Laplace transform technique. The effects of parameters such as magnetic parameter, porous matrix, thermal and mass buoyancy parameters, thermal radiation, heat absorption parameter, radiation conduction parameter, Prandtl and Schmidt numbers and the homogeneous chemical reaction are shown via graphs. The results for the physical quantities of interest such as the rate of shear stress and the rate of heat and mass transfer coefficients are also obtained and presented through graphs. Observing these, the emerging role of a few parameters is elaborated in the results and discussion section.

Keywords. Free convection; nanofluids; radiation absorption; heat and mass transfer; Laplace transformation.

PACS Nos **44.05.+e; 44.25.+f; 44.40.+a**

1. Introduction

Since a few decades, nanofluids have been used in many industrial and engineering applications, thermal diffusion and chemical reactions because of the significance of buoyancy effects caused by heat and mass transfer. For that reason, the combined effects of heat and the solutal transfer of nanofluids can be used in various engineering applications such as energy transport, automobiles, coolants, electronics and combination, polymer production, environmental pollution and for maintaining moisture over cultivated fields. Many researchers have conducted studies and have reported that the boundary layer flow of the heat and mass transfer of conducting fluids have many applications in industrial technology, manufacturing and developmental processes which include the cooling of electronic devices by the motor cooling of nuclear reactors throughout emergency shutdown, manufacturing of plastics and rubber sheets, textile and paper industries, glass-fibre production, plasmas studies, boundary layer control in the field of aerodynamics and in the flow of biological fluids. Choi [1] was the first to use the word 'nanofluid' to denote a fluid in which nanoparticles are floated. Its importance is appreciated in various applications in geophysics and astrophysics [2]. Sarpkaya [3] had studied the usefulness of magnetohydrodynamics (MHD) in non-Newtonian fluids. Current studies concerning the flow phenomena in diverse situations are discussed in [4–11]. Alternatively, radiative heat transfer has been used in various applications, e.g. missiles and aircraft, nuclear power plants, propulsion devices for space vehicles, gas turbines, etc. Furthermore, the effect of the reactant species also attracted the attention of many scientists owing to their extensive role in industries. Gireesha *et al* [12,13] discussed various effects on the flow phenomena when fluids over a stretched surface were fixed in a non-Darcy porous medium. In their study, a non-uniform heat source/sink was taken into consideration in the energy equation. Pal and Talukdar

[14] have investigated the flow past a vertical permeable plate. The velocity and concentration profiles decrease when the reactant species and heat radiation increases. Chamkha [15] clearly illustrated the numerical exploration of the effect of reactant substance in his study. Furthermore, Uwanta and Omokhuale [16] revisited the work with a viscoelastic fluid in a stationary plane. Ramana Reddy *et al* [17] studied the influence of magnetic field on flow past a vertical oscillating plate in a porous medium. Sulochana *et al* [18] cross-examined the boundary layer behaviour of flows through dissipative effect. In recent times, Rashid *et al* [19] studied the existence of thermal radiation effects on Casson fluid past the stretching surface. The knowledge of chemical reaction is useful in fields of engineering and technology, viz., polymer processing, chemical industries, glass manufacturing industry, food processing, etc. By using Laplace transform technique, Das *et al* [20] and Bhattacharyya and Layek [21] explained the influence of chemical reaction when the flow is along a vertical plate. Later, many investigators [22–25] studied the flow of nanofluid between two parallel plates under the influence of chemically reacting species. They testified that nanoparticle volume fraction in collaboration with Eckert number is directly related to the Nusselt number. When two plates are detached, Nusselt number has an inverse relationship with the squeeze number when double plates are squeezed. Furthermore, Sheikholeslami and Ganji [26] and Sheikholeslami *et al* [27] worked on MHD natural convection heat transfer in an inclined L-shaped cavity. They showed that the augmentation in heat energy transfer has an opposite correlation with Rayleigh number and Hartmann number. Saleh [28] and Mahanthesh *et al* [29] investigated the flow phenomena of nanofluids past a vertical plate. Das and Jana [30] studied the radiative heat transfer past a moving vertical plate. Baag and Mishra [31] illustrated the MHD 3D water-based nanofluid of heat transfer. Rout and Mishra [32] recently explored heat transfer phenomena on MHD nanofluid flow over a stretching surface. Baag *et al* [33] examined the magnetohydrodynamic boundary layer flow over a stretching sheet past a porous medium through a constant heat source. Mishra and Rout [34] discussed the MHD KKL model nanofluid past a stretching sheet. A study on hybrid nanofluids over a vertical surface in the presence of radiative heat energy and the heat source/sink was conducted by Ashlin and Mahanthesh [35]. Gireesha *et al* [36] recently presented a topic on the Casson nanofluid effect on chemical reactions. Furthermore, Mahanthesh and Gireesha [37,38] and Mahanthesh *et al* [39–43] have investigated their work on various nanofluids in different geometries.

Owing to the aforesaid discussion about the literature surface, our study aims at the role of radiation absorption which affects the heat transfer phenomenon of various nanofluid flows. In addition to that, mass buoyancy through a porous matrix which enhances the fluid motion is incorporated in the momentum equation. Depending upon the physical situation, we have also studied the mass transfer effect which was neglected in the earlier study of Mahanthesh *et al* [29]. The main attraction of the present paper is the analytical solution of the complex nonlinear partial differential equations. The solution to these equations is obtained by employing Laplace transform technique. The present result validates with earlier established result and found to be in good agreement in particular cases.

2. Formalism

Unsteady nanofluid flow on a moving/stationary perpendicular flat plate has been investigated. The governing equation of continuity, momentum, energy and concentration of nanofluids are discussed:

$$\nabla \cdot U = 0, \tag{1}$$

$$\rho_{\mathrm{nf}} \frac{\partial U}{\partial t} = -\nabla p + \mu_{\mathrm{nf}} \nabla^2 U + J \times B + gb, \tag{2}$$

$$\left(\rho c_p\right)_{\mathrm{nf}} \frac{\partial T}{\partial t} = -\nabla \cdot q, \tag{3}$$

$$\frac{\partial C}{\partial t} = -\nabla \cdot j, \tag{4}$$

where $U = (u, v, w)$, $q = -k_{\mathrm{nf}} \nabla T$ is the heat flux, $j = -D\nabla C$ is the mass flux and $J = \sigma_{\mathrm{nf}}(E + U \times B)$ is the current density. u, v, w are the velocity components along x, y and z direction respectively.

The flow is in the vertical x direction, which is along the plate and y-axis is normal to it, i.e. the plane $y = 0$ and the plate overlap. Here, $y > 0$ represents the existence of flow, as presented in figure 1. B_0 is the strength of the magnetic field, which is applied to the transverse direction of the flow and the radiative heat flux q_{r} is also considered using Rosseland approximations. Here, it is considered that the pressure gradient is isolated, where the electrically conducting water-based nanofluid is considered with the metal copper (Cu) and metal oxide (TiO_2) as nanoparticles. In addition, it is deliberated that the host fluid and deferred nanoparticles are thermally stable. Following Saleh [28], the governing equations with the corresponding surface conditions are

$$\rho_{\mathrm{nf}} \frac{\partial u}{\partial t} = \mu_{\mathrm{nf}} \frac{\partial^2 u}{\partial y^2} - \sigma_{\mathrm{nf}} B_0^2 u + g(\rho\beta_T)_{\mathrm{nf}}(T - T_\infty) + g(\rho\beta_C)_{\mathrm{nf}}(C - C_\infty) - \frac{\mu_{\mathrm{nf}} u}{K}, \tag{5}$$

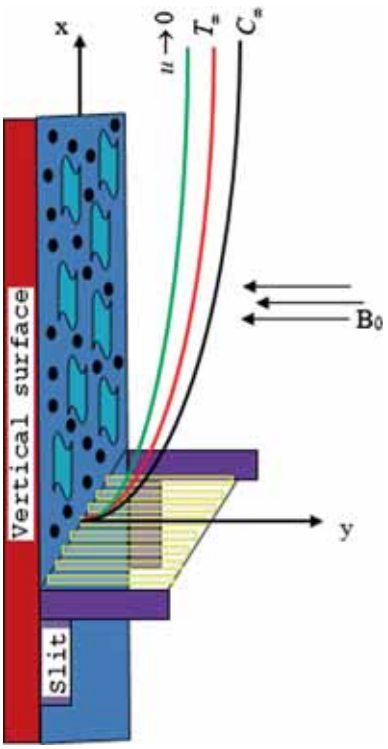

Figure 1. Geometrical configuration.

$$\left(\rho c_p\right)_{\mathrm{nf}}\frac{\partial T}{\partial t} = k_{\mathrm{nf}}\frac{\partial^2 T}{\partial y^2} - \frac{\partial q_{\mathrm{r}}}{\partial y} + Q_0(T - T_\infty) + Q_1(C - C_\infty), \tag{6}$$

$$\frac{\partial C}{\partial t} = D\frac{\partial^2 C}{\partial y^2} - k_1(C - C_\infty), \tag{7}$$

$$\left.\begin{array}{llll} t = 0: u = 0, & T = T_\infty, & C = C_\infty, & \forall y \geq 0 \\ t > 0: u = \lambda u_0, & T = T_{\mathrm{w}}, & C = C_{\mathrm{w}} & \text{at } y = 0 \\ t > 0: u \to 0, & T = T_\infty, & C = C_{\mathrm{w}} & \text{as } y \to \infty \end{array}\right\}, \tag{8}$$

where the plate moves linearly with velocity u_0. Here, $\lambda \neq 0$ represents the plate being stationary and $\lambda = 0$ represents the plate under the moving condition. In the above set of equations, ρ_{nf} is the nanofluid density, λ is the direction of plate movement, B_0 is the magnetic field strength, g is the gravitational force, β_T is the thermal expansion coefficient, T is the fluid temperature, T_∞ is the temperature away from the wall, T_{w} is the wall temperature, t is the time, C is the fluid concentration, C_∞ is the concentration away from the wall.

Following Das and Jana [30], the effective properties of nanofluids are given as follows:

$$\rho_{\mathrm{nf}} = (1-\phi)\rho_{\mathrm{f}} + \phi\rho_{\mathrm{s}}, \quad \mu_{\mathrm{nf}} = \frac{\mu_f}{(1-\phi)^{2.5}},$$
$$(\rho c_p)_{\mathrm{nf}} = (1-\phi)(\rho c_p)_{\mathrm{f}} + \phi(\rho c_p)_{\mathrm{s}},$$
$$(\rho\beta_T)_{\mathrm{nf}} = (1-\phi)(\rho\beta_T)_{\mathrm{f}} + \phi(\rho\beta_T)_{\mathrm{s}},$$
$$(\rho\beta_C)_{\mathrm{nf}} = (1-\phi)(\rho\beta_C)_{\mathrm{f}} + \phi(\rho\beta_C)_{\mathrm{s}},$$
$$\sigma_{\mathrm{nf}} = \sigma_{\mathrm{f}}\left[1 + \frac{3(\sigma_{\mathrm{s}}/\sigma_{\mathrm{f}} - 1)\phi}{(\sigma_{\mathrm{s}}/\sigma_{\mathrm{f}} + 2) - (\sigma_{\mathrm{s}}/\sigma_{\mathrm{f}} - 1)\phi}\right],$$
$$k_{\mathrm{nf}} = k_{\mathrm{f}}\left\{\frac{k_{\mathrm{s}} + 2k_{\mathrm{f}} - 2\phi(k_{\mathrm{f}} - k_{\mathrm{s}})}{k_{\mathrm{s}} + 2k_{\mathrm{f}} + 2\phi(k_{\mathrm{f}} - k_{\mathrm{s}})}\right\}.$$

where ϕ is the volume fraction. Now by using Rosseland approximation, and following Hayat *et al* [25], the radiative heat flux q_{r} can be expressed as

$$q_{\mathrm{r}} = -\frac{4\sigma^*}{k^*}\frac{\partial T^4}{\partial y}.$$

Using the Taylor series expansion of T^4 about T_∞ and neglecting the higher-order term, we get

$$T^4 \approx 4T_\infty^3 T - 3T_\infty^4.$$

In view of the above description, eq. (6) is of the form

$$\left(\rho c_p\right)_{\mathrm{nf}}\frac{\partial T}{\partial t} = k_{\mathrm{nf}}\frac{\partial^2 T}{\partial y^2} + \frac{16T_\infty^3\sigma^*}{3k^*}\frac{\partial^2 T}{\partial y^2} + Q_0(T - T_\infty) + Q_1(C - C_\infty). \tag{9}$$

With the help of the following non-dimensional quantities:

$$\eta = \frac{u_0 y}{\nu_{\mathrm{f}}}, \quad \tau = \frac{u_0^2 t}{\nu_{\mathrm{f}}}, \quad f = \frac{u}{u_0},$$
$$\theta(\eta) = \frac{T - T_\infty}{T_{\mathrm{w}} - T_\infty}, \quad \psi = \frac{C - C_\infty}{C_{\mathrm{w}} - C_\infty},$$
$$M^2 = \frac{\sigma_{\mathrm{f}} B_0 \nu_{\mathrm{f}}}{u_0\rho_{\mathrm{f}}}, \quad \mathrm{Gr} = \frac{g\beta_{\mathrm{Tf}}(T_{\mathrm{w}} - T_\infty)\nu_{\mathrm{f}}}{u_0^3},$$
$$\mathrm{Gc} = \frac{g\beta_{\mathrm{Cf}}(C_{\mathrm{w}} - C_\infty)\nu_{\mathrm{f}}}{u_0^3}$$
$$\mathrm{Pr} = \frac{(\mu c_p)_{\mathrm{f}}}{k_{\mathrm{f}}}, \quad R = \frac{4\sigma^* T_\infty^3}{k^* k_{\mathrm{f}}}, \quad Q = \frac{Q_0\nu_{\mathrm{f}}}{u_0^2(\rho c_p)_{\mathrm{f}}},$$
$$\mathrm{Sc} = \frac{D}{\nu_{\mathrm{f}}}, \quad K = \frac{k_1\nu_{\mathrm{f}}}{u_0^2},$$

where θ is the temperature profile, ψ is the concentration profile, Gr is the thermal Grashof number, Gc is the solute Grashof number, ν_{f} is the kinematic viscosity of fluid, Pr is the Prandtl number, R is the radiation parameter, k^* is the mean absorption coefficient, Q is the heat generation/absorption, u_0 is a constant, Sc is the generalized Schmidt number, D is the mass diffusion coefficient. Substituting in eqs (5), (7), (8) and (9) we get

$$\frac{\partial f}{\partial \tau} = r_1\frac{\partial^2 f}{\partial \eta^2} + r_2\,\mathrm{Gr}\,\theta + r_3\,\mathrm{Gc}\,\psi - r_4 M f, \tag{10}$$

$$\frac{\partial \theta}{\partial \tau} = r_5\frac{\partial^2 f}{\partial \eta^2} + r_6\theta, \tag{11}$$

$$\frac{\partial\psi}{\partial\tau} = \frac{1}{\mathrm{Sc}}\frac{\partial^2\psi}{\partial\eta^2} - K\psi, \tag{12}$$

$$\left.\begin{array}{l} \tau = 0: \quad f = 0, \quad \theta = 0, \quad \psi = 0 \quad \forall\eta \geq 0 \\ \tau > 0: \left\{\begin{array}{l} f = \lambda, \ \theta = 1, \quad \psi = 1 \quad \text{at}\ \eta \geq 0 \\ f \to 0, \ \theta \to 0, \ \psi \to 0 \quad \text{as}\ \eta \to \infty \end{array}\right. \end{array}\right\}. \tag{13}$$

where f is the dimentionless velocity component.

3. Solution methodology

The solution of eqs (10)–(12) with the given boundary conditions (13) is obtained analytically. We have employed the Laplace transformation technique. By applying Laplace transform on both sides of eqs (10)–(13), we get

$$r_1\frac{\mathrm{d}^2\bar{f}}{\mathrm{d}\eta^2} + r_2\,\mathrm{Gr}\,\bar{\theta} + r_3\,\mathrm{Gc}\,\bar{\psi} - (r_4M^2 + s)\,\bar{f} = 0, \tag{14}$$

$$r_5\frac{\mathrm{d}^2\bar{\theta}}{\mathrm{d}\eta^2} + (r_6 - s)\bar{\theta} = 0, \tag{15}$$

$$\frac{1}{\mathrm{Sc}}\frac{\mathrm{d}^2\bar{\psi}}{\mathrm{d}\eta^2} - (K + s)\bar{\psi} = 0 \tag{16}$$

$$\left.\begin{array}{l} \bar{f} = 0, \ \bar{\theta} = 0, \ \bar{\psi} = 0, \quad \forall\eta \geq 0 \\ \bar{f} = \frac{\lambda}{s}, \ \bar{\theta} = \frac{1}{s}, \ \bar{\psi} = \frac{1}{s} \ \text{at}\ \eta = 0 \\ \bar{f} \to 0, \bar{\theta} \to 0, \bar{\psi} \to 0 \ \text{as}\ \eta \to \infty \end{array}\right\}. \tag{17}$$

Now eqs (14)–(16) are purely ordinary differential equations with some initial and boundary conditions presented in (17) which can be solved easily and we get the following equations:

$$\bar{\psi}(s,\eta) = \frac{1}{s}\mathrm{e}^{-\sqrt{\mathrm{Sc}(s+k_\mathrm{c})}\eta},$$

$$\psi(t,\eta) = \frac{1}{2}\left\{\mathrm{e}^{\sqrt{\mathrm{Sc}k_\mathrm{c}}\eta}\mathrm{erfc}\left(\frac{\sqrt{\mathrm{Sc}}\eta}{2\sqrt{t}} + \sqrt{k_\mathrm{c}t}\right) + \mathrm{e}^{-\sqrt{\mathrm{Sc}k_\mathrm{c}}\eta}\mathrm{erfc}\left(\frac{\sqrt{\mathrm{Sc}}\eta}{2\sqrt{r_5t}} - \sqrt{k_\mathrm{c}t}\right)\right\},$$

$$\bar{\theta}(s,\eta) = \frac{1}{s}\mathrm{e}^{(1/\sqrt{r_5})\sqrt{s-r_6}\eta} + r_{10}\left[\frac{\mathrm{e}^{-\sqrt{\mathrm{Sc}(s+k_\mathrm{c})}\eta}}{s} - \frac{\mathrm{e}^{-\sqrt{\mathrm{Sc}(s+k_\mathrm{c})}\eta}}{s+r_9} - \frac{\mathrm{e}^{-(1/\sqrt{r_5})\sqrt{S(s-r_6)}\eta}}{s} + \frac{\mathrm{e}^{-(1/\sqrt{r_5})\sqrt{S(s-r_6)}\eta}}{s+r_9}\right],$$

$$\begin{aligned}\theta(t,\eta) &= \frac{1}{2}\left\{\mathrm{e}^{\sqrt{(-r_6/r_5)}\eta}\mathrm{erfc}\left(\frac{\eta}{2\sqrt{r_5t}} + \sqrt{-r_6t}\right) + \mathrm{e}^{-\sqrt{(-r_6/r_5)}\eta}\mathrm{erfc}\left(\frac{\eta}{2\sqrt{r_5t}} - \sqrt{-r_6t}\right)\right\} \\ &+ r_{10}\left[\frac{1}{2}\left\{\mathrm{e}^{\sqrt{\mathrm{Sc}k_\mathrm{c}}\eta}\mathrm{erfc}\left(\frac{\sqrt{\mathrm{Sc}}\eta}{2\sqrt{t}} + \sqrt{k_\mathrm{c}t}\right) + \mathrm{e}^{-\sqrt{\mathrm{Sc}k_\mathrm{c}}\eta}\mathrm{erfc}\left(\frac{\sqrt{\mathrm{Sc}}\eta}{2\sqrt{r_5t}} - \sqrt{k_\mathrm{c}t}\right)\right\}\right. \\ &- \mathrm{e}^{-r_9t}\left\{\mathrm{e}^{\sqrt{\mathrm{Sc}(k_\mathrm{c}-r_9)}\eta}\mathrm{erfc}\left(\frac{\sqrt{\mathrm{Sc}}\eta}{2\sqrt{t}} + \sqrt{(k_\mathrm{c}-r_9)t}\right) + \mathrm{e}^{-\sqrt{\mathrm{Sc}(k_\mathrm{c}-r_9)}\eta}\mathrm{erfc}\left(\frac{\sqrt{\mathrm{Sc}}\eta}{2\sqrt{t}} - \sqrt{(k_\mathrm{c}-r_9)t}\right)\right\} \\ &- \frac{1}{2}\left\{\mathrm{e}^{\sqrt{(-r_6/r_5)}\eta}\mathrm{erfc}\left(\frac{\eta}{2\sqrt{r_5t}} + \sqrt{-r_6t}\right) + \mathrm{e}^{-\sqrt{(-r_6/r_5)}\eta}\mathrm{erfc}\left(\frac{\eta}{2\sqrt{r_5t}} - \sqrt{-r_6t}\right)\right\} \\ &+ \frac{\mathrm{e}^{-r_9t}}{2}\left\{\mathrm{e}^{\sqrt{(-r_6-r_9/r_5)}\eta}\mathrm{erfc}\left(\frac{\eta}{2\sqrt{r_5t}} + \sqrt{-r_6-r_9t}\right) + \mathrm{e}^{-\sqrt{(-r_6/r_5)}\eta}\mathrm{erfc}\left(\frac{\eta}{2\sqrt{r_5t}} - \sqrt{-r_6-r_9t}\right)\right\}\Bigg],\end{aligned}$$

$$\begin{aligned}f(t,\eta) &= \frac{\lambda}{2}\left\{\mathrm{e}^{\sqrt{\frac{A}{r_1}}\eta}\mathrm{erfc}\left(\frac{\eta}{2\sqrt{r_1t}} + \sqrt{At}\right) + \mathrm{e}^{-\sqrt{\frac{A}{r_1}}\eta}\mathrm{erfc}\left(\frac{\eta}{2\sqrt{r_1t}} - \sqrt{At}\right)\right\} \\ &- \frac{r_{26}}{2}\mathrm{e}^{r_{13}t}\left\{\mathrm{e}^{\sqrt{\frac{A+r_{13}}{r_1}}\eta}\mathrm{erfc}\left(\frac{\eta}{2\sqrt{r_1t}} + \sqrt{(A+r_{13})t}\right) + \mathrm{e}^{-\sqrt{\frac{A+r_{13}}{r_1}}\eta}\mathrm{erfc}\left(\frac{\eta}{2\sqrt{r_1t}} - \sqrt{(A+r_{13})t}\right)\right\} \\ &- \frac{r_{26}}{2}\left\{\mathrm{e}^{\sqrt{\frac{A}{r_1}}\eta}\mathrm{erfc}\left(\frac{\eta}{2\sqrt{r_1t}} + \sqrt{At}\right) + \mathrm{e}^{-\sqrt{\frac{A}{r_1}}\eta}\mathrm{erfc}\left(\frac{\eta}{2\sqrt{r_1t}} - \sqrt{At}\right)\right\} \\ &+ \frac{r_{19}}{2}\left\{\mathrm{e}^{\sqrt{\frac{A}{r_1}}\eta}\mathrm{erfc}\left(\frac{\eta}{2\sqrt{r_1t}} + \sqrt{At}\right) + \mathrm{e}^{-\sqrt{\frac{A}{r_1}}\eta}\mathrm{erfc}\left(\frac{\eta}{2\sqrt{r_1t}} - \sqrt{At}\right)\right\} \\ &+ \frac{r_{20}}{2}\mathrm{e}^{-r_9t}\left\{\mathrm{e}^{\sqrt{\frac{A-r_9}{r_1}}\eta}\mathrm{erfc}\left(\frac{\eta}{2\sqrt{r_1t}} + \sqrt{(A-r_9)t}\right) + \mathrm{e}^{-\sqrt{\frac{A-r_9}{r_1}}\eta}\mathrm{erfc}\left(\frac{\eta}{2\sqrt{r_1t}} - \sqrt{(A-r_9)t}\right)\right\} \\ &+ \frac{r_{21}}{2}\mathrm{e}^{-r_{15}t}\left\{\mathrm{e}^{\sqrt{\frac{A-r_{15}}{r_1}}\eta}\mathrm{erfc}\left(\frac{\eta}{2\sqrt{r_1t}} + \sqrt{(A-r_{15})t}\right)\right.\end{aligned}$$

$$+\mathrm{e}^{-\sqrt{\frac{A-r_{15}}{r_1}}\eta}\operatorname{erfc}\left(\frac{\eta}{2\sqrt{r_1 t}}-\sqrt{(A-r_{15})t}\right)\Bigg\}$$
$$+\frac{r_{22}}{2}\Bigg\{\mathrm{e}^{\sqrt{\frac{A}{r_1}}\eta}\operatorname{erfc}\left(\frac{\eta}{2\sqrt{r_1 t}}+\sqrt{At}\right)$$
$$+\mathrm{e}^{-\sqrt{\frac{A}{r_1}}\eta}\operatorname{erfc}\left(\frac{\eta}{2\sqrt{r_1 t}}-\sqrt{At}\right)\Bigg\}$$
$$+\frac{r_{23}}{2}\mathrm{e}^{-r_9 t}\Bigg\{\mathrm{e}^{\sqrt{\frac{A-r_9}{r_1}}\eta}\operatorname{erfc}\left(\frac{\eta}{2\sqrt{r_1 t}}+\sqrt{(A-r_9)t}\right)$$
$$+\mathrm{e}^{-\sqrt{\frac{A-r_9}{r_1}}\eta}\operatorname{erfc}\left(\frac{\eta}{2\sqrt{r_1 t}}-\sqrt{(A-r_9)t}\right)\Bigg\}$$
$$+\frac{r_{24}}{2}\mathrm{e}^{r_{13}t}\Bigg\{\mathrm{e}^{\sqrt{\frac{A+r_{13}}{r_1}}\eta}\operatorname{erfc}\left(\frac{\eta}{2\sqrt{r_1 t}}+\sqrt{(A+r_{13})t}\right)$$
$$+\mathrm{e}^{-\sqrt{\frac{A-r_9}{r_1}}\eta}\operatorname{erfc}\left(\frac{\eta}{2\sqrt{r_1 t}}-\sqrt{(A-r_{13})t}\right)\Bigg\}$$

$$+\frac{r_{25}}{2}\mathrm{e}^{r_{18}t}\Bigg\{\mathrm{e}^{\sqrt{\frac{A+r_{18}}{r_1}}\eta}\operatorname{erfc}\left(\frac{\eta}{2\sqrt{r_1 t}}+\sqrt{(A+r_{18})t}\right)$$
$$+\mathrm{e}^{-\sqrt{\frac{A-r_{18}}{r_1}}\eta}\operatorname{erfc}\left(\frac{\eta}{2\sqrt{r_1 t}}-\sqrt{(A-r_{18})t}\right)\Bigg\}$$
$$-\frac{r_{25}}{2}\Bigg\{\mathrm{e}^{\sqrt{\frac{A}{r_1}}\eta}\operatorname{erfc}\left(\frac{\eta}{2\sqrt{r_1 t}}+\sqrt{At}\right)$$
$$+\mathrm{e}^{-\sqrt{\frac{A}{r_1}}\eta}\operatorname{erfc}\left(\frac{\eta}{2\sqrt{r_1 t}}-\sqrt{At}\right)\Bigg\}$$
$$+\frac{r_{26}}{2}\mathrm{e}^{r_{13}t}\Bigg\{\mathrm{e}^{\sqrt{\frac{-r_6+r_{13}}{r_5}}\eta}$$
$$\times\operatorname{erfc}\left(\frac{\eta}{2\sqrt{r_5 t}}+\sqrt{(-r_6+r_{13})t}\right)$$
$$+\mathrm{e}^{-\sqrt{\frac{-r_6+r_{13}}{r_5}}\eta}\operatorname{erfc}\left(\frac{\eta}{2\sqrt{r_5 t}}-\sqrt{(-r_6+r_{13})t}\right)\Bigg\}$$
$$-\frac{r_{26}}{2}\Bigg\{\mathrm{e}^{\sqrt{\frac{-r_6}{r_5}}\eta}\operatorname{erfc}\left(\frac{\eta}{2\sqrt{r_5 t}}+\sqrt{-r_6 t}\right)$$
$$+\mathrm{e}^{-\sqrt{\frac{-r_6}{r_5}}\eta}\operatorname{erfc}\left(\frac{\eta}{2\sqrt{r_5 t}}-\sqrt{-r_6 t}\right)\Bigg\}$$
$$-\frac{r_{19}}{2}\mathrm{e}^{r_{13}t}\Bigg\{\mathrm{e}^{\sqrt{\mathrm{Sc}k_c}\eta}\operatorname{erfc}\left(\frac{\sqrt{\mathrm{Sc}}\eta}{2\sqrt{r_5 t}}+\sqrt{k_c t}\right)$$
$$+\mathrm{e}^{-\sqrt{\mathrm{Sc}k_c}\eta}\operatorname{erfc}\left(\frac{\sqrt{\mathrm{Sc}}\eta}{2\sqrt{r_5 t}}-\sqrt{k_c t}\right)\Bigg\}$$
$$-\frac{r_{20}}{2}\mathrm{e}^{-r_9 t}\Bigg\{\mathrm{e}^{\sqrt{\mathrm{Sc}(k_c-r_9)}\eta}$$
$$\times\operatorname{erfc}\left(\frac{\sqrt{\mathrm{Sc}}\eta}{2\sqrt{t}}+\sqrt{(k_c-r_9)t}\right)$$
$$+\mathrm{e}^{-\sqrt{\mathrm{Sc}(k_c-r_9)}\eta}\operatorname{erfc}\left(\frac{\sqrt{\mathrm{Sc}}\eta}{2\sqrt{t}}-\sqrt{(k_c-r_9)t}\right)\Bigg\}$$
$$-\frac{r_{21}}{2}\mathrm{e}^{-r_{15}t}\Bigg\{\mathrm{e}^{\sqrt{\mathrm{Sc}(k_c-r_{15})}\eta}$$
$$\times\operatorname{erfc}\left(\frac{\sqrt{\mathrm{Sc}}\eta}{2\sqrt{t}}+\sqrt{(k_c-r_{15})t}\right)$$
$$+\mathrm{e}^{-\sqrt{\mathrm{Sc}(k_c-r_{15})}\eta}\operatorname{erfc}\left(\frac{\sqrt{\mathrm{Sc}}\eta}{2\sqrt{t}}-\sqrt{(k_c-r_{15})t}\right)\Bigg\}$$
$$-\frac{r_{22}}{2}\Bigg\{\mathrm{e}^{\sqrt{\frac{-r_6}{r_5}}\eta}\operatorname{erfc}\left(\frac{\eta}{2\sqrt{r_5 t}}+\sqrt{-r_6 t}\right)$$
$$+\mathrm{e}^{-\sqrt{\frac{-r_6}{r_5}}\eta}\operatorname{erfc}\left(\frac{\eta}{2\sqrt{r_5 t}}-\sqrt{-r_6 t}\right)\Bigg\}$$
$$-\frac{r_{23}}{2}\mathrm{e}^{-r_9 t}\Bigg\{\mathrm{e}^{\sqrt{\frac{-r_6-r_9}{r_5}}\eta}$$
$$\times\operatorname{erfc}\left(\frac{\eta}{2\sqrt{r_5 t}}+\sqrt{(-r_6-r_9)t}\right)$$
$$+\mathrm{e}^{-\sqrt{\frac{-r_6-r_9}{r_5}}\eta}\operatorname{erfc}\left(\frac{\eta}{2\sqrt{r_5 t}}-\sqrt{(-r_6-r_9)t}\right)\Bigg\}$$
$$-\frac{r_{24}}{2}\mathrm{e}^{r_{13}t}\Bigg\{\mathrm{e}^{\sqrt{\frac{-r_6+r_{13}}{r_5}}\eta}$$
$$\times\operatorname{erfc}\left(\frac{\eta}{2\sqrt{r_5 t}}+\sqrt{(-r_6+r_{13})t}\right)$$
$$+\mathrm{e}^{-\sqrt{\frac{-r_6+r_{13}}{r_5}}\eta}\operatorname{erfc}\left(\frac{\eta}{2\sqrt{r_5 t}}-\sqrt{(-r_6+r_{13})t}\right)\Bigg\}$$
$$-\frac{r_{25}}{2}\mathrm{e}^{r_{18}t}\Bigg\{\mathrm{e}^{\sqrt{\mathrm{Sc}(k_c+r_{18})}\eta}$$
$$\times\operatorname{erfc}\left(\frac{\sqrt{\mathrm{Sc}}\eta}{2\sqrt{t}}+\sqrt{(k_c+r_{18})t}\right)$$
$$+\mathrm{e}^{-\sqrt{\mathrm{Sc}(k_c+r_{18})}\eta}\operatorname{erfc}\left(\frac{\sqrt{\mathrm{Sc}}\eta}{2\sqrt{t}}-\sqrt{(k_c+r_{18})t}\right)\Bigg\}$$
$$+\frac{r_{25}}{2}\mathrm{e}^{r_{18}t}\Bigg\{\mathrm{e}^{\sqrt{\mathrm{Sc}k_c}\eta}\operatorname{erfc}\left(\frac{\sqrt{\mathrm{Sc}}\eta}{2\sqrt{t}}+\sqrt{k_c t}\right)$$
$$+\mathrm{e}^{-\sqrt{\mathrm{Sc}k_c}\eta}\operatorname{erfc}\left(\frac{\sqrt{\mathrm{Sc}}\eta}{2\sqrt{t}}-\sqrt{k_c t}\right)\Bigg\}.$$

All constants are presented in the Appendix.

4. Results and discussion

The free convective flow of water-based nanofluids with Cu and TiO_2 nanoparticles past a moving vertical plate is investigated. An electrically conducting fluid passing through a porous medium in the presence of thermal radiation and radiation conduction parameter is the crux of the present study. The nonlinear differential equations are solved analytically by

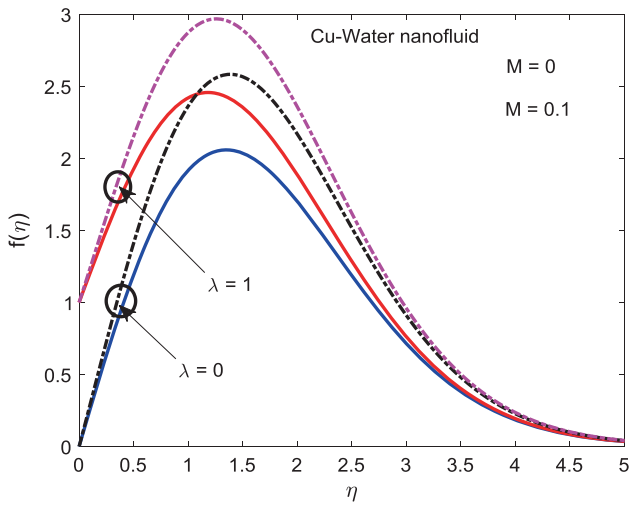

Figure 2. Comparison plot of the Cu–water nanofluid velocity profile for $K_p = 0, p = 0.1$, Gr $= 10$, $Q_1 = 0$, Gc $= 10$, Pr $= 1$, $R = 0.1, Q_0 = 0.1$, Sc $= 0.2$ and $K_c = 1$.

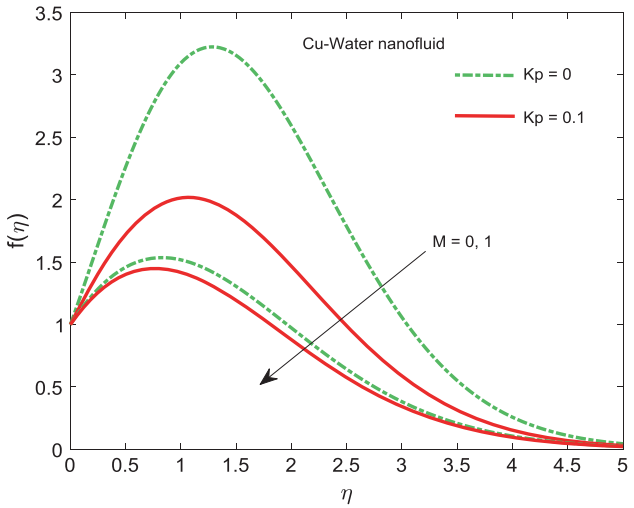

Figure 3. Influence of magnetic parameter and porous matrix on the velocity profiles of the Cu–water nanofluid for $\phi = 0.1$, Gr $=$ Gc $= 10$, $Q_1 =$ Pr $= K_c = 1, R = 0.1$, $Q_0 = 0.1$ and Sc $= 0.2$.

employing Laplace transformation. The behaviour of several embedding parameters on the flow phenomena with the thermophysical properties of nanoparticles and water was investigated and presented through figures 2–12. The validation of the present results with the results of Sheikholeslami and Ganji [26] and Sheikholeslami *et al* [27] were obtained and the results are excellent. Throughout the discussion, we have taken water as the base fluid with copper (Cu) and titanium oxide (TiO_2) nanoparticles and the physical properties of these particles are shown in figures 13–16 *vis-à-vis* the results for the Nusselt and Sherwood numbers are calculated.

4.1 *Velocity distributions*

Figure 2 displays the validation of the present work with the result of Mahanthesh *et al* [29] when the magnetic parameter $M = 0$, the porous matrix $K_p = 0$, the heat source parameter $Q = 0$ and the chemical reaction parameter $K_c = 0$ when the plate is stationary, i.e. $\lambda = 0$. Also, in the presence of all the aforementioned parameters and in the absence of radiation absorption parameter Q_1 ($Q_1 = 0$), the said observation agrees well with the work of Mahanthesh *et al* [29]. Furthermore, from figure 2, it is noteworthy that retardation in the momentum of the Cu–water nanofluid is marked for $M \neq 0$ and $K_p = 0$ in the velocity boundary layer when the plate is either stationary ($\lambda = 0$) or under the moving condition ($\lambda \neq 0$). This is the usual phenomenon of the interference of the magnetic parameter in the fluid motion, and the fact is, the inclusion of the magnetic parameter produces Lorentz force which is a resistive force that has a significant role in retarding the velocity profile. When the plate is under the moving condition, the velocity of the nanofluid increases rapidly near the plate within the region $\eta < 1.5$ which decreases the boundary layer thickness, and afterwards, it decreases smoothly to meet the boundary condition. The influence of the porous matrix in the presence/absence of the magnetic parameter is displayed in figure 3. The absence of both parameters was described earlier in figure 2. The presence of the porous matrix in both the presence/absence of the magnetic parameter decreases the nanofluid velocity also. As the magnetic parameter interference of the porous matrix also resists the velocity significantly, it can be clearly noticed that the maximum velocity in the velocity profile is exhibited by withdrawing the porous matrix which coincides with the work of Sheikholeslami and Ganji [26] and Sheikholeslami *et al* [27]. Figure 4 displays the influence of the magnetic parameter and the porous matrix on the velocity profile of the TiO_2–water nanofluid. The effect is very similar to that of figure 3 described earlier but in comparison with figure 3, it can be clearly observed that the TiO_2–water based nanofluid has more viscous effect than that of the Cu–water nanofluid as the profiles are very close to each other in figure 4 than in figure 3. The effect of the thermal buoyancy parameter Gr and mass buoyancy parameter Gc on the TiO_2–water nanofluid velocity profile are shown in figures 5 and 6, respectively, in the presence/absence of a porous matrix. Here, Gr > 0, Gc > 0 represent the assisting flow and Gr < 0, Gc < 0 represent the opposing one. In both figures, the assisting flow enhances the fluid velocity, whereas the opposing one has a reverse effect on it. From figure 5, it is evident

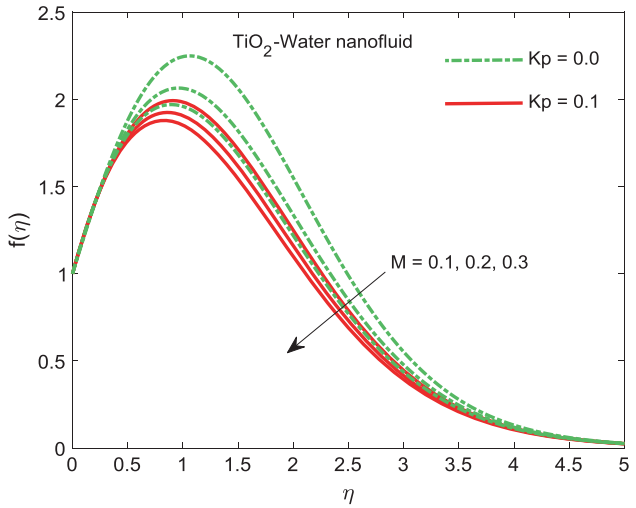

Figure 4. Influence of magnetic parameter and porous matrix on the velocity profiles of the TiO_2–water nanofluid for $\phi = 0.1$, $\mathrm{Gr} = \mathrm{Gc} = 10$, $Q_1 = \mathrm{Pr} = K_c = 1$, $R = 0.1$, $Q_0 = 0.1$ and $\mathrm{Sc} = 0.2$.

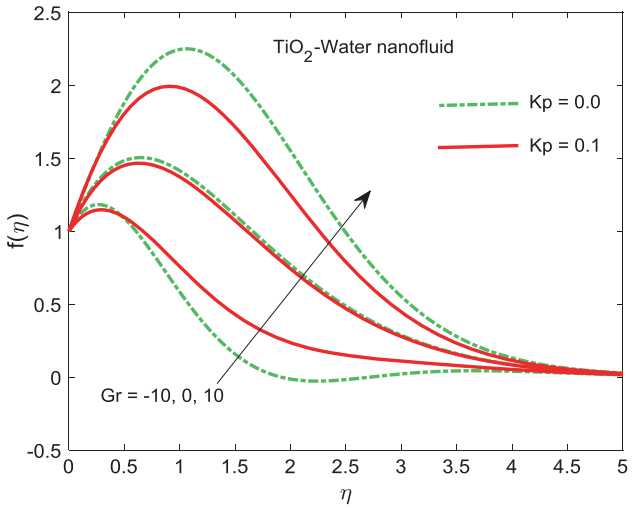

Figure 5. Influence of thermal buoyancy and porous matrix on the velocity profiles of the TiO_2–water nanofluid for $M = 0.1$, $\phi = 0.1$, $Q_1 = 1$, $\mathrm{Gc} = 10$, $\mathrm{Pr} = 1$, $R = 0.1$, $Q_0 = 0.1$, $\mathrm{Sc} = 0.2$ and $K_c = 1$.

that in both the assisting and the opposing flows, there is a rapid growth in the velocity profile near the plate within the region $\eta < 1.5$, and afterwards, it decreases. In figure 6, the case of the assisting flow, growth is observed near the plate within the region $\eta < 0.5$ but flow instability is marked in the case of the opposing flow. In the case of the opposing flow, the velocity profile retards near the plate. It is also noticed that in the absence of the porous matrix, the velocity of the TiO_2–water based nanofluid is the maximum near the plate. Further, the presence of porous matrix decreases the momentum in the presence/absence of porous matrix.

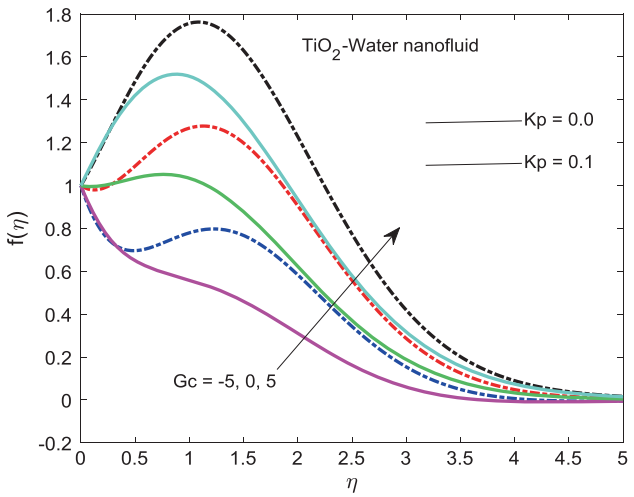

Figure 6. Influence of solutal buoyancy and porous matrix on the velocity profiles of the TiO_2–water nanofluid for $M = 0.1$, $\phi = 0.1$, $Q_1 = 1$, $\mathrm{Gr} = 10$, $\mathrm{Pr} = 1$, $R = 0.1$, $Q_0 = 0.1$, $\mathrm{Sc} = 0.2$ and $K_c = 1$.

4.2 *Temperature distributions*

Figure 7 shows the comparison plot for the temperature distribution in the absence of the radiation absorption parameter. Also, the variation of the solid volume fraction for different time periods is exhibited in the profile. For $t = 0.1$ and in the case of pure fluid ($\phi = 0$) (marked as red dotted line), the present result validates the work of Mahanthesh *et al* [29]. It is observed that the increase in volume fraction with the increase in time enhances the temperature of the Cu–water nanofluid in the thermal boundary layer because of the inclusion of both magnetic and porous matrices. The resistive forces which have retarding effects on the velocity distribution described earlier, resist the fluid motion which is favourable to enhance the temperature profile. The profile is asymptotic in nature. Figure 8 displays the effect of radiation absorption parameter on the temperature profiles of both Cu–water and TiO_2–water nanofluids. In the absence of radiation absorption parameter, both the profiles have the same magnitude and coincide with each other. However, increasing values of Q_1 enhance the fluid temperature. It is clear that the variation of Cu and TiO_2 nanofluids are insignificant, but the hike in temperature is remarkable in the case of the TiO_2 nanofluid. Many manufacturing industries require a particular type of nanofluid for the production of materials at the time of cooling. The influence of the heat sink parameter Q in the absence/presence of the radiation absorption parameter Q_1 is shown in figure 9. In the absence of both radiation absorption and sink parameters, the results of

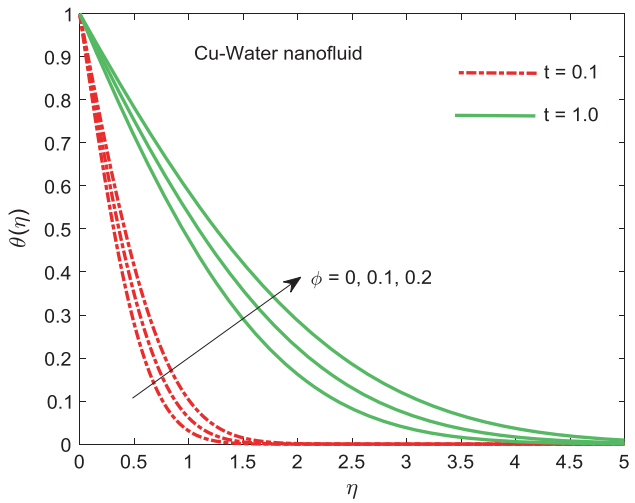

Figure 7. Influence of volume fraction and t on the temperature profile of the Cu–water nanofluid for $Q_1 = 0, \mathrm{Pr} = 1, R = 0.1, Q_0 = -0.1, \mathrm{Sc} = 0.22$ and $K_c = 1$.

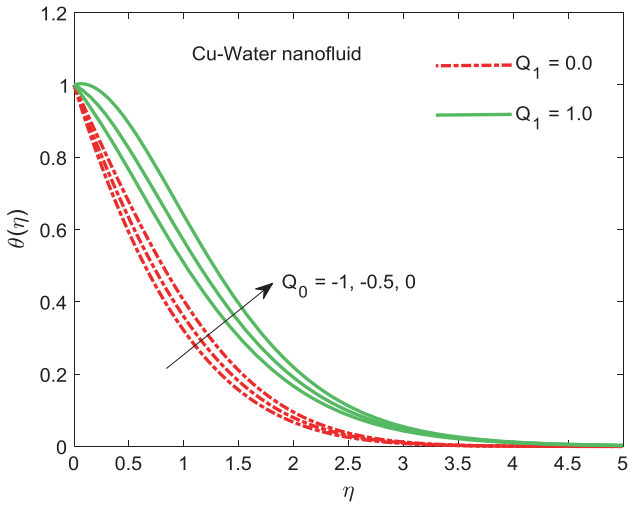

Figure 9. Influence of heat sink parameter on the Cu–water nanofluid temperature profiles for $M = 0.1, \phi = 0.1$, $\mathrm{Gr} = \mathrm{Gc} = 10, \mathrm{Pr} = K_c = 1, R = 0.1, Q_1 = 10$ and $\mathrm{Sc} = 0.2$.

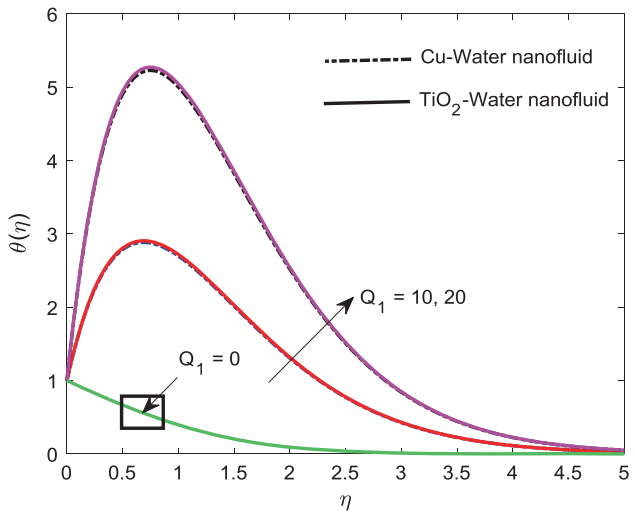

Figure 8. Influence of radiation absorption on both Cu–water and TiO_2–water nanofluid temperature profiles for $M = 0.1, \phi = 0.1, \mathrm{Gr} = \mathrm{Gc} = 10, \mathrm{Pr} = K_c = 1, R = 0.1$, $Q_0 = 0.1$ and $\mathrm{Sc} = 0.2$.

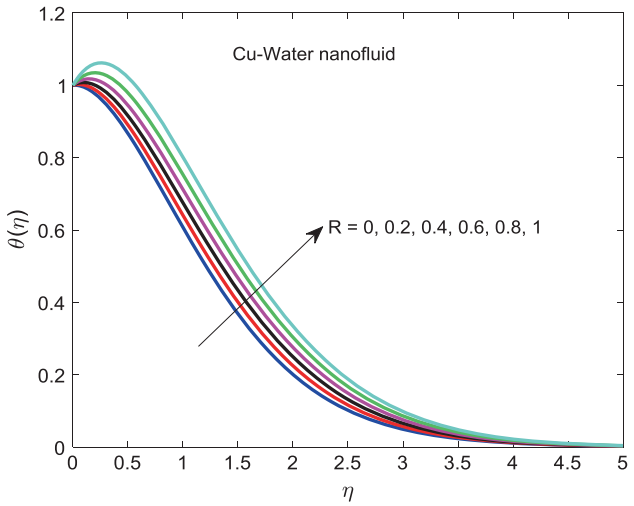

Figure 10. Influence of thermal radiation on the Cu–water nanofluid temperature profiles for $M = 0.1, \phi = 0.1$, $\mathrm{Gr} = \mathrm{Gc} = 10, \mathrm{Pr} = K_c = 1, Q_1 = 10, Q_0 = 0.1$ and $\mathrm{Sc} = 0.2$.

Mahanthesh *et al* [29] coincide with the current result. Furthermore, it is noteworthy that the heat-sink in both the absence/presence of the radiation absorption parameter decreases the nanofluid temperature. However, with an increase in the absorption coefficient, the fluid temperature increases significantly. Figure 10 portrays the influence of radiative heat on the temperature distribution of the Cu–water nanofluid. 'Thermal radiation is the electromagnetic transfer of energy from a hotter surface to a colder surface and thus represents heat transfer without a physical medium' [28]. Therefore, an increase in thermal radiation increases the Cu–water nanofluid temperature. Also, Cu is a good conductor of heat which enhances the thermal boundary layer thickness at all points in its boundary layer.

4.3 *Concentration distributions*

Figures 11 and 12 exhibit the effects of a destructive chemical reaction parameter along with Schmidt number on the concentration profiles of the Cu–water and TiO_2–water nanofluids. It can be clearly observed that in the absence of the chemical reaction parameter, the concentration value is the maximum with a low

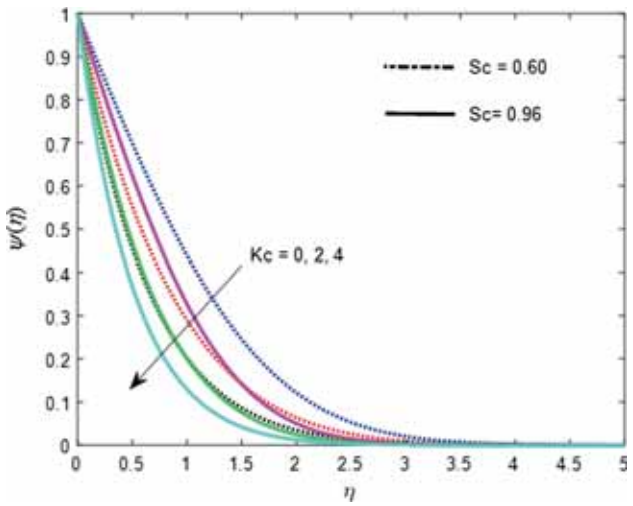

Figure 11. Influence of Schmidt number and chemical reaction parameter on the Cu–water nanofluid concentration profiles for $M = 0.1, \phi = 0.1, \text{Gr} = \text{Gc} = 10$, $\text{Pr} = 1$, $R = 0.1$, $Q_1 = 1$, $Q_0 = 0.1$ and $t = 0.5$.

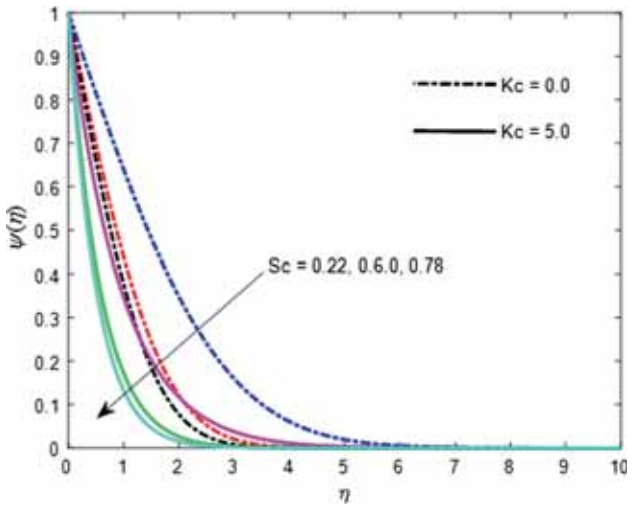

Figure 12. Influence of Schmidt number and chemical reaction parameter on the Cu–water nanofluid concentration profiles for $M = 0.1, \phi = 0.1, \text{Gr} = \text{Gc} = 10$, $\text{Pr} = 1$, $R = 0.1$, $Q_1 = 1$, $Q_0 = 0.1$ and $t = 0.5$.

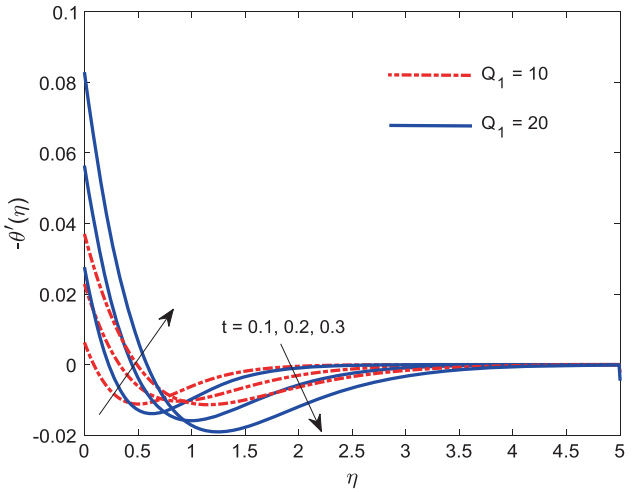

Figure 13. Influence of radiation absorption and t on the rate of heat transfer of the Cu–water nanofluid for $M = 0.1, \phi = 0.1, \text{Gr} = \text{Gc} = 10, \text{Pr} = 1, R = 0.1$ and $Q_0 = 0.1$.

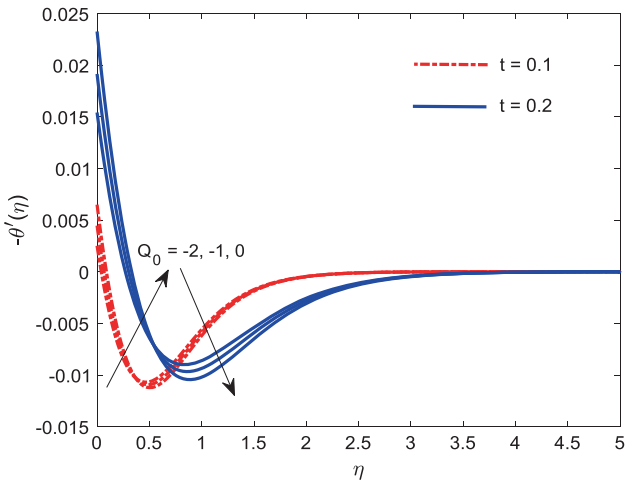

Figure 14. Influence of heat sink and t on the rate of heat transfer of the Cu–water nanofluid for $M = 0.1, \phi = 0.1, \text{Gr} = \text{Gc} = 10, \text{Pr} = 1, R = 0.1$ and $Q_1 = 1$.

Schmidt number. However, the heavier species and the destructive chemical reaction retard the nanofluid concentration in the solutal boundary layer, resulting in a decrease in the solutal boundary layer thickness.

4.4 *Results of engineering interest*

Finally, figures 13–16 present the engineering interests via the Nusselt number and the Sherwood number for various values of physical parameters. In figure 13, a sharp fall in the rate of heat transfer is marked near the plate within the region $\eta < 0.75$ and afterwards the effect is reversed. Also, it is observed that with an increase in time period t, the Nusselt number increases in the first region presented earlier and further decreases as well. The radiation absorption parameter has a similar tendency on the rate of heat transfer. It is interesting to note that only the heat sink has a significant role in the profile. Mathematical evidence is that the heat source is not suitable for the expression of the rate of heat transfer. Again, figure 14 displays the variation of heat sink and time t on the rate of heat transfer profile. For $t = 0.1$, the sharp fall in the profile is marked within a region $\eta < 0.5$ and for $t = 0.2$ the fall is marked

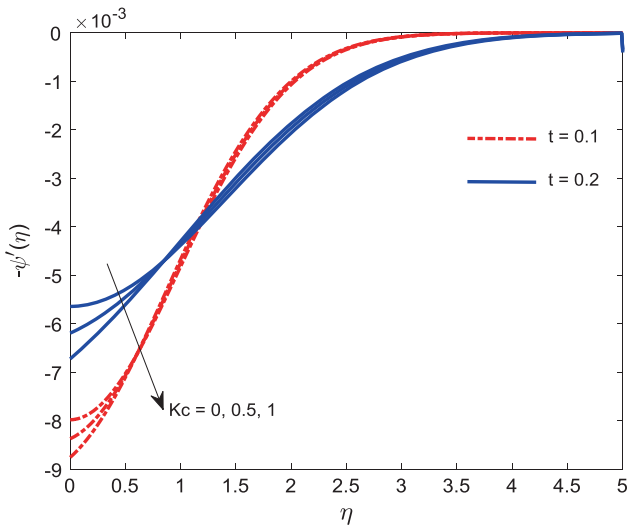

Figure 15. Influence of chemical reaction and t on the rate of mass transfer of the Cu–water nanofluid for $M = 0.1, \phi = 0.1, \text{Gr} = \text{Gc} = 10, \text{Pr} = 1, R = 0.1$ and $Q_1 = 1$.

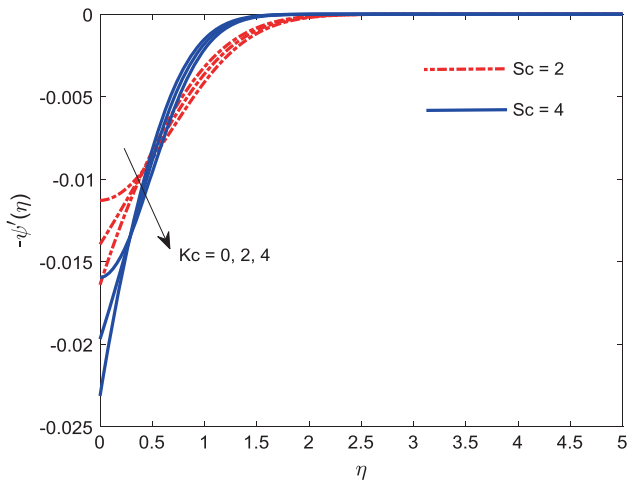

Figure 16. Influence of chemical reaction and Schmidt number on the rate of mass transfer of the Cu–water nanofluid for $M = 0.1, \phi = 0.1, \text{Gr} = \text{Gc} = 10, \text{Pr} = 1, R = 0.1$ and $Q_1 = 1$.

within the region $\eta < 1.0$. Moreover, the sink decreases the Nusselt number in the first region, and further, the result is insignificant. The rate of solutal transfer for various values of chemical reaction parameter and time t of the Cu–water nanofluid is displayed in figure 15. It is observed that for $t = 0.1$, the rate of increase is rapid from negative to meet the required boundary condition. However, for $t = 0.2$, the rate of increase is slower. But there is no increase in the chemical reaction of the profile, i.e., the mass transfer rate coefficient decreases. This decrease is more significant for $t = 0.2$. It is also observed that the character is distinct in two different regions from the point of infection for $t = 0.2$, i.e. $\eta < 1.0$ and $\eta > 1.0$. When $\eta < 1.0$, the profile decreases with the increasing value of chemical reaction parameter. However, when $\eta > 1.0$, the effect is reversed. The influence of chemical reaction parameter and heavier species on the rate of mass transfer of the Cu–water nanofluid is exhibited in figure 16. The effect of K_c is described earlier in figure 15. However, the heavier species which retards the concentration profile as described in figure 12 has a vital role on the mass transfer rate. When $\text{Sc} = 2$, the coefficient has a higher rate within the region $\eta < 0.5$ and for higher species, i.e. $\text{Sc} = 4$, the coefficient decreases in the region where $\eta > 0.5$. Therefore, it can be concluded that heavier species is used to control the solutal rate which may be beneficial for the shape of the final product in industries.

5. Conclusion

The analytical solution of free convective flow of nanofluids over a vertical plate is obtained in this paper. The presence of thermal radiation and radiation conduction parameter enhances the study as well. In addition to that, the electrically conducting nanofluid passing through a porous medium also affects the flow phenomena. The non-dimensional form of nonlinear partial differential equations is solved by employing the Laplace transformation technique. The effect of various parameters characterising the flow phenomena are presented and discussed. A few major findings are given here:

- Porous matrix in collaboration with the magnetic parameter diminishes the Cu–water nanofluid velocity profile.
- Enhancement in the velocity profile is marked in the case of the assisting case and the opposing case retards it significantly.
- An increase in radiation absorption increases the nanofluid temperature.
- Thermal radiation is beneficial to hike the nanofluid temperature as Cu is a good conductor of heat.
- Heavier species in the presence of the chemical reaction parameter retards nanofluid concentration.
- Radiation absorption augmented with the heat sink increases the heat transfer rate.

Last but not least, the present study presents a wide range of applications and warrants a further study on nanofluids.

Appendix

$$x_1 = (1-\phi) + \phi\frac{\rho_s}{\rho_f}, \quad x_2 = (1-\phi) + \phi\frac{(\rho\beta_T)_s}{(\rho\beta_T)_f},$$
$$x_3 = (1-\phi) + \phi\frac{(\rho\beta_C)_s}{(\rho\beta_C)_f},$$
$$x_4 = \left[1 + \frac{3(\sigma-1)\phi}{\sigma+2-(\sigma-1)\phi}\right],$$
$$\sigma = \frac{\sigma_s}{\sigma_f}, \quad x_5 = (1-\phi) + \phi\frac{(\rho c_p)_s}{(\rho c_p)_f},$$
$$x_6 = \frac{k_{nf}}{k_f} = \left[\frac{k_s + 2k_f - 2k\phi(k_f - k_s)}{k_s + 2k_f + \phi(k_f - k_s)}\right],$$
$$r_1 = \frac{1}{(1-\phi)^{2.5}x_1}, \quad r_2 = \frac{x_2}{x_1},$$
$$r_3 = \frac{x_3}{x_1}, \quad r_4 = \frac{x_4}{x_1}, \quad r_5 = \frac{1}{x_5\,\mathrm{Pr}}\left\{x_6 + \frac{3}{4}R\right\},$$
$$r_6 = \frac{Q}{x_5}, \quad r_7 = \frac{Q^*}{x_5}, \quad r_8 = \frac{r_7}{(r_5\,\mathrm{Sc}-1)},$$
$$r_9 = \frac{r_5 k_c + r_6}{r_5\,\mathrm{Sc}-1}, \quad r_{10} = \frac{r_8}{r_9},$$
$$r_{11} = \frac{r_1}{r_5}, \quad r_{12} = \frac{r_2\,\mathrm{Gr}}{r_{11}-1},$$
$$r_{13} = \frac{r_6 r_{11} + m^2 r_4 + (r_1/k_p)}{r_{11}-1},$$
$$A = m^2 r_4 + \frac{r_1}{k_p}, \quad r_{14} = \frac{\mathrm{Gr}\,r_2 r_8}{r_1\mathrm{Sc}-1},$$
$$r_{15} = \frac{r_1\,\mathrm{Sc}(A-k_c)}{r_1\,\mathrm{Sc}-1}, \quad r_{16} = \frac{\mathrm{Gr}\,r_2 r_8}{r_{11}-1},$$
$$r_{17} = \frac{\mathrm{Gc}\,r_3}{r_1\,\mathrm{Sc}-1}, \quad r_{18} = \frac{r_1\,\mathrm{Sc}\,k_c - A}{r_1\,\mathrm{Sc}-1}, \quad r_{19} = \frac{r_{14}}{r_9 r_{15}},$$
$$r_{20} = -\frac{r_{14}}{r_9(r_{15}-r_9)}, \quad r_{21} = -\frac{r_{14}}{r_{15}(r_9-r_{15})},$$
$$r_{22} = \frac{r_{16}}{r_9 r_{13}}, \quad r_{23} = -\frac{r_{16}}{r_9(r_{13}+r_9)},$$
$$r_{24} = -\frac{r_{16}}{r_{13}(r_9+r_{13})}, \quad r_{25} = \frac{r_{17}}{r_{18}}, \quad r_{26} = \frac{r_{12}}{r_{13}}.$$

References

[1] S Choi, *Developments and applications of non-Newtonian flows* edited by D A Siginer and H P Wang (ASME, New York, 1995) FED-vol. 231/MD-vol. 66, p. 99

[2] W F Huges and F J Yong, *The electro-magneto-dynamics of fluids* (John Wiley and Sons, New York, USA, 1966)

[3] T Sarpkaya, *AIChE J.* **7**, 324 (1961)

[4] H A Attia and K M Ewis, *Tamkang J. Sci. Eng.* **13** (**4**), 359 (2010)

[5] M E Sayed-Ahmedand and H A Attia, *Int. Commun. Heat Mass Transf.* **27**(**8**), 1177 (2000)

[6] T Hayat and O U Mehmood, *Commun. Nonlinear Sci. Numer. Simul.* **16**(**3**), 1363 (2011)

[7] M Modather, A M Rashad and A J Chamkha, *Turk. J. Eng. Environ. Sci.* **33**, 245 (2009)

[8] S Nadeem, M Hussain and M Naz, *Int. J. Meccanica* **45**, 869 (2010)

[9] B K Jha and C A Apere, *Appl. Math. Model.* **37**, 1920 (2013)

[10] O D Makinde and T Chinyoka, *Comput. Math. Appl.* **60**, 660 (2010)

[11] B J Gireesha, B Mahanthesh and M M Rashidi, *Int. J. Ind. Math.* **7**, 14 (2015)

[12] B J Gireesha, B Mahanthesh, P T Manjunatha and R S R Gorla, *J. Niger. Math. Soc.* **34**(**3**), 267 (2015)

[13] B J Gireesha, B Mahanthesh, R S R Gorla and P T Manjunatha, *Heat Mass Transf.* **52(4)**, 897 (2016)

[14] D Pal and B Talukdar, *Commun. Nonlinear Sci. Numer. Simul.* **15**(**7**), 1813 (2010)

[15] A J Chamkha, *Int. Commun. Heat Mass Transf.* **30**(**3**), 413 (2003)

[16] I J Uwanta and E Omokhuale, *Res. J. Math. Stat.* **4**(**3**), 63 (2012)

[17] J V Ramana Reddy, V Sugunamma and N Sandeep, *J. Adv. Phys.* **5**, 295 (2017)

[18] C Sulochana, S P Samrat and N Sandeep, *Int. J. Mech. Sci.* **128–129**, 326 (2017)

[19] M Rashid, S Rana, N S Akbar and S Nadeem, *Alexandria Eng. J.* (2017), https://doi.org/10.1016/J.aej.2017.01.010, in press

[20] U N Das, R Deka and V M Soundalgekar, *Forsch. Im Ingenieurwesen-Eng. Res.* **60**, 284 (1994)

[21] K Bhattacharyya and G C Layek, *Meccanica* **47**, 1043 (2012)

[22] C Sulochana, G P Ashwinkumar and N Sandeep, *Int. J. Adv. Sci. Technol.* **86**, 61 (2016)

[23] C Sulochana, M K Kishor Kumar and N Sandeep, *Chem. Process Eng. Res.* **37**, 24 (2015)

[24] N Sandeep, C Sulochana and L A Isaac, *Int. J. Eng. Res. Africa.* **20**, 93 (2016)

[25] T Hayat, M Rashid, M Imtiaz and A Alsaedi, *J. Mol. Liq.* **225**, 482 (2017)

[26] M Sheikholeslami and D D Ganji, *Powder Technol.* **235**, 873 (2013)

[27] M Sheikholeslami, D D Ganji and M Gorji-Bandpy, *J. Taiwan Inst. Chem. Eng.* **45(4)**, 1204 (2014)

[28] J Saleh, *Fluid flow handbook* (McGraw-Hill, New York, 2002) p. 27.5

[29] B Mahanthesh, B J Gireesha and R S R Gorla, *Alexandria Eng. J.* **55**, 569 (2016)

[30] S Das and R N Jana, *Alex. Eng. J.* **54**, 55 (2015)

[31] S Baag and S R Mishra, *J. Nanofluid* **4**(**3**), 1 (2015)

[32] B C Rout and S R Mishra, *Eng. Sci. Technol. Int. J.* **21**(**1**), 60 (2018)

[33] S Baag, S R Mishra, M M Hoque and N N Anika, *J. Nanofluids* **7**(**3**), 570 (2018)
[34] S R Mishra and B C Rout *Iran, J. Sci. Technol. Trans. Sci.* **43(3)**, 1239 (2019)
[35] S Ashlin and B Mahanthesh, *J. Nanofluids* **8**, 781 (2019)
[36] B J Gireesha, M Archana, B Mahanthesh and B C Prasannakumara, *Multidiscip. Model. Mater. Struct.* **15**(**1**), 227 (2019)
[37] B Mahanthesh and B J Gireesha, *Results Phys.* **8**, 869 (2018)
[38] B Mahanthesh and B J Gireesha, *Results Phys.* **8**, 537 (2018)
[39] B Mahanthesh, B J Gireesha, B C Prasannakumara and N S Shashikumar, *Nucl. Eng. Technol.* **49**(**8**), 1660 (2017)
[40] B Mahanthesh, B J Gireesha, N S Shashikumar and S A Shehzad, *Physica E* **94**, 25 (2017)
[41] B Mahanthesh, B J Gireesha, S A Shehzad, A Rauf and P B S Kumar, *Physica B* **537**, 98 (2018)
[42] B Mahanthesh, B J Gireesha, M Sheikholeslami, S A Shehzad and P B S Kumar, *J. Nanofluids* **7**(**6**), 1089 (2018)
[43] B J Gireesha, P B Sampath Kumar and B Mahanthesh, *Microgravity Sci. Technol.* **30**(**3**), 257 (2018)